



Bulk growth, electrical, linear, third order nonlinear optical and optical limiting properties on bis(cyclohexylammonium) succinate succinic acid crystal

R. Gomathi, S. Madeswaran*, D. Rajan Babu

Department of Physics, School of Advanced Sciences, Vellore Institute of Technology, Vellore, 632014, Tamil Nadu, India

HIGHLIGHTS

- BCSSA crystal with dimensions of $10 \times 4 \times 3 \text{ mm}^3$ was grown by solution growth method.
- The dielectric properties were analyzed and discussed.
- Electrical conductivity was calculated for BCSSA crystal.
- Optical band gap of BCSSA was found to be 4.9 eV.
- Z-scan analysis reveals the high nonlinear efficiency and optical limiting property of the crystal.

ARTICLE INFO

Article history:

Keywords:

Crystal growth
Optical material
Z-scan technique
Dielectrics
Optical limiting properties

ABSTRACT

Organic material of bis(cyclohexylammonium) succinate succinic acid (BCSSA) single crystal was grown by slow evaporation technique at room temperature and bulk of BCSSA was grown by slow cooling method. Single crystal XRD analysis reveals that the BCSSA crystal belongs to the triclinic crystal system with centro-symmetric space group ($P\bar{1}$). The FT-IR spectrum confirms the functional groups of NH_3^+ , succinate and succinic acid present in the BCSSA crystal, showing the evidence of compound formation and optical band gap was calculated using UV-Vis-NIR analysis. The third order nonlinear optical parameters were calculated by Z scan technique using 532 nm diode pumped CW Nd:YAG Laser and the optical limiting spectrum of BCSSA shows the suitability in optical limiting applications.

© 2017 Elsevier B.V. All rights reserved.

1. Introduction

Organic materials are essential for various nonlinear optical applications such as high speed information processing, waveguide fabrication, optical communications and optical storage [1,2]. As compared to inorganic counterpart, organic materials are attracting a great attention due to their large nonlinear optical efficiencies and offering a large number of possibilities [3]. Organic crystals contain highly delocalized π electrons, electron donor and acceptor groups which give large nonlinear optical and electro optic effects [4,5]. Dicarboxylic acids are the versatile building blocks which can create numerous possibilities through the formation of hydrogen bonded networks [6]. Succinic acid generally exists in neutral state (succinic acid) or in ionized state (succinate) [7,8]. The bis

(cyclohexylammonium) succinate succinic acid (BCSSA) salt adduct has been crystallized in triclinic crystal structure with two cyclohexylammonium cations, one succinate dianion and one neutral succinic acid molecule ($2\text{C}_6\text{H}_{14}\text{N}^+ \cdot \text{C}_4\text{H}_4\text{O}_4^{2-} \cdot \text{C}_4\text{H}_6\text{O}_4$). The crystal structure of BCSSA was solved by Modou Sarr et al. [9]. The succinate dianion and succinic acid neutral molecules are connecting in head to tail through O-H-O hydrogen bond. The carboxyl-carboxylate dianion adopts a syn-syn configuration, thus prominent a strand arrangement. Cyclohexylammonium cations act as multidentate hydrogen bond donors, joining adjacent strands through N-H-O interactions of both succinate and succinic acid components resulting two dimensional supramolecular networks. In the present investigation we have reported the crystal growth, FT-IR analysis, dielectric studies, linear optical, third order nonlinear optical studies, chemical etching and limiting response of BCSSA crystal.

* Corresponding author.

E-mail address: madeswaran.s@vit.ac.in (S. Madeswaran).

2. Experimental work

2.1. Synthesis and bulk crystal growth

BCSSA single crystal was obtained from the mixed solution of cyclohexylamine (5.76 mL, Sigma Aldrich with 99% purity) and succinic acid (5.0 g, Sigma Aldrich with 99% purity) in 50 mL of water as followed by the previous report [9]. The solution was stirred well continuously for twenty hours to get a homogeneous solution. After attaining the homogeneity, the solution was filtered in a beaker using wattman filter paper and it was covered with transparent polyethylene cover. The solution was slowly evaporated at room temperature. After a period of three weeks colorless crystals were harvested from the solution. Fig. 1 (a) shows the as grown crystal of BCSSA material ($10 \times 4 \times 3 \text{ mm}^3$). Purification of material is important step for organic crystal growth. BCSSA crystal was purified by repeated recrystallization in water. The solubility of BCSSA was gravimetrically analyzed in the range of 30–50 °C and Fig. 1 (b) shows that the BCSSA crystal exhibits positive temperature gradient. Since the temperature is stabilized throughout the period, a good quality transparent (strain and defect free) bulk crystal was grown by slow cooling technique. At first 43.62 g of BCSSA was dissolved in 100 mL of water at 35 °C using constant temperature bath (0.01 °C accuracy) and continuously stirred well for 6 h. The seed crystal of BCSSA was tied into that solution and the temperature was reduced 0.1 °C per day. After a period of 35 days a colorless transparent crystal with dimension of $26 \times 9 \times 3 \text{ mm}^3$ harvested from the solution which is shown in Fig. 1 (c).

3. Results and discussion

3.1. Single crystal XRD analysis

The lattice parameters of BCSSA crystal were determined using single crystal XRD (Enraf Norius CAD4 diffractometer with MoK α radiation) analysis at 293 K. The cell parameters are $a = 9.640$ (2) (Å), $b = 10.514$ (11) (Å), $c = 11.433$ (2) (Å), $\alpha = 96.76$ (4)°, $\beta = 93.38$ (2)°, $\gamma = 90.99$ (5)° and the volume is 1147.6 (3) (Å³). The structure of BCSSA is triclinic centro-symmetric P $\bar{1}$ space group. These values are well agreed with the previous report [9]. The density of grown crystal was calculated using the

formula [10],

$$\rho = \frac{zM}{NV} \text{g/cm}^3 \quad (1)$$

where, z is the number of formula units in one unit cell ($z = 2$), M is atomic mass in grams, N is Avogadro number and V is volume in centimeter cube. The density was calculated around 1.283 g/cm^3 . The solid state parameters such as plasma energy, pen gap, Fermi gap energy and polarizability were calculated using single crystal XRD and dielectric measurement and the value of polarizability was compared with theoretical value calculated from Clausius-Mossotti equation. The valence electron plasma energy was calculated using [11],

$$\hbar\omega_p = 28.8 \left[\frac{Z\rho}{M} \right]^{1/2} \quad (2)$$

where, Z is the total number of valence electrons ($Z = 192$), ρ is density and M is molecular weight of the crystal. The Penn gap and the Fermi energy expressed in terms of $\hbar\omega_p$ are given by,

$$E_p = \frac{\hbar\omega_p}{(\epsilon_\infty - 1)^{1/2}} \quad (3)$$

where, ϵ_∞ is the dielectric constant of the material at higher frequency.

$$E_F = 0.2948(\hbar\omega_p)^{4/3} \quad (4)$$

The molecular polarizability (α) is obtained using the relation [19],

$$\alpha = \left[\left(\frac{(\hbar\omega_p)^2 S_0}{(\hbar\omega_p)^2 S_0 + 3E_p^2} \right) \right] \times \frac{M}{\rho} \times 0.396 \times 10^{-24} \text{ cm}^{-1} \quad (5)$$

where, S_0 is the constant for particular material and is given by Ref. [17],

$$S_0 = 1 - \left[\frac{E_p}{4E_F} \right] + \frac{1}{3} \left[\frac{E_p}{4E_F} \right]^2 \quad (6)$$

The value of α also obtained using Clausius-Mossotti equation which is given by Ref. [11],

$$\alpha = \frac{3M}{4\pi N\rho} \left(\frac{\epsilon_\infty - 1}{\epsilon_\infty + 2} \right) \quad (7)$$

The obtained values are presented in Table 1. The obtained value of large polarizability is the responsible for high third order NLO properties which agrees with Z-scan measurements [23].

3.2. FT-IR analysis

The presence of functional group in BCSSA was confirmed by FT-

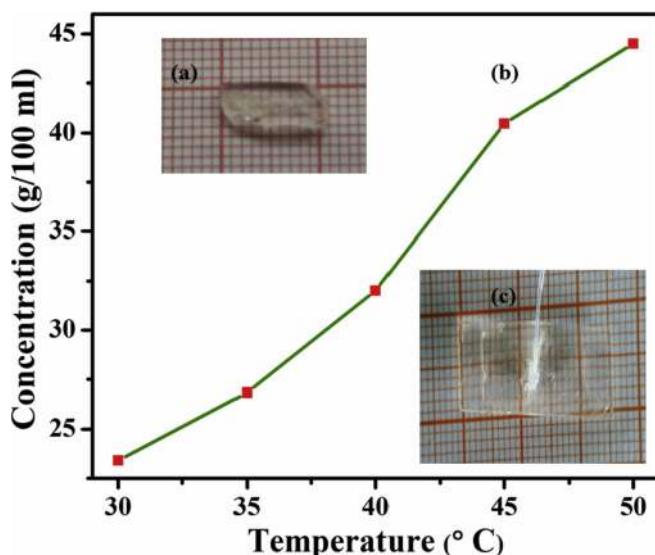


Fig. 1. (a) As grown crystal. (b) solubility curve and (c) bulk growth of BCSSA.

Table 1
Theoretical measurements of BCSSA crystal.

Parameter	Values
Plasma energy	21.68 eV
Penn gap energy	2.04 eV
Fermi energy	17.82 eV
Polarizability	
By Penn analysis	$13.05 \times 10^{-23} \text{ cm}^3$
By Clausius-Mossotti equation	$13.08 \times 10^{-23} \text{ cm}^3$

IR analysis in the range of 400–4000 cm^{-1} using SHMADZU IR Affinity-1s spectrometer (shown in Fig. 2). The peaks at 2941.44 cm^{-1} , 2549.89 cm^{-1} and 1527.62 cm^{-1} represent the NH_3^+ in plane symmetric stretching and NH_3^+ asymmetric bending respectively. The presence of C=O group of saturated free acid was represented by the peak at 1710.86 cm^{-1} [12]. The bands observed at 2860.43 cm^{-1} and 1128.36 cm^{-1} were due to the C-H symmetric stretching and C-H in plane bending [13]. As a whole the spectrum establishes the presence of protonated NH_3^+ and free acid in that compound. The functional groups and their assignments are shown in Table 2.

3.3. Optical studies

The transmittance window is an important characteristic of a nonlinear optical material. The UV-Vis-NIR spectrum of BCSSA was shown in Fig. 3 (a) (200–800 nm) and the characteristic absorption band is observed at 238 nm. It is due to the electronic transition of $n-\pi^*$ caused by carboxylic group present in the compound. The absorption coefficient (α) was calculated using the transmittance value (T) [14],

$$\alpha = \frac{2.3026 \log(1/T)}{t} \quad (8)$$

where, t is the thickness of the sample. The optical band gap (E_g) was calculated using the following relation [15],

$$\alpha h\nu = A(h\nu - E_g)^{1/2} \quad (9)$$

Where, A is a constant, h is plank constant and ν is the frequency of incident photons. From Fig. 3 (b), the band gap was obtained by extrapolating the linear portion of absorption edge to energy axis and it is found to be 4.9 eV.

Table 2
Molecular vibrational assignments of BCSSA Compound.

Wavenumber (cm^{-1})	Assignments
2941.44–2549.89	NH_3^+ in plane symmetric stretching
2860.43	C-H Symmetric stretching
1710.86	C=O groups of saturated free acid
1625.99 & 1379.10	COO^- Stretching
1527.62	NH_3^+ Asymmetric bending
1234.44	C-O Stretching vibration
1128.36	C-N Asymmetric stretching
1022.27	C-N Symmetric stretching
800.46	COO^- Rocking
711.73	COO^- Scissoring
632.65	COO^- Wagging
516.92	C-C=O Wagging

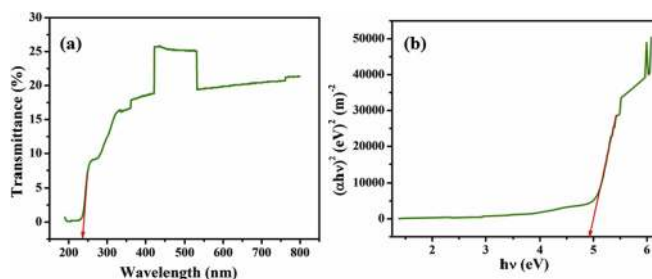


Fig. 3. (a) Transmittance spectrum and (b) Tauc's plot.

3.4. Electrical studies

Dielectric studies reveal the nature of atoms and a measure of ability of the polarizable ions with electric field distribution within the crystal [16]. The dielectric measurements of BCSSA were carried

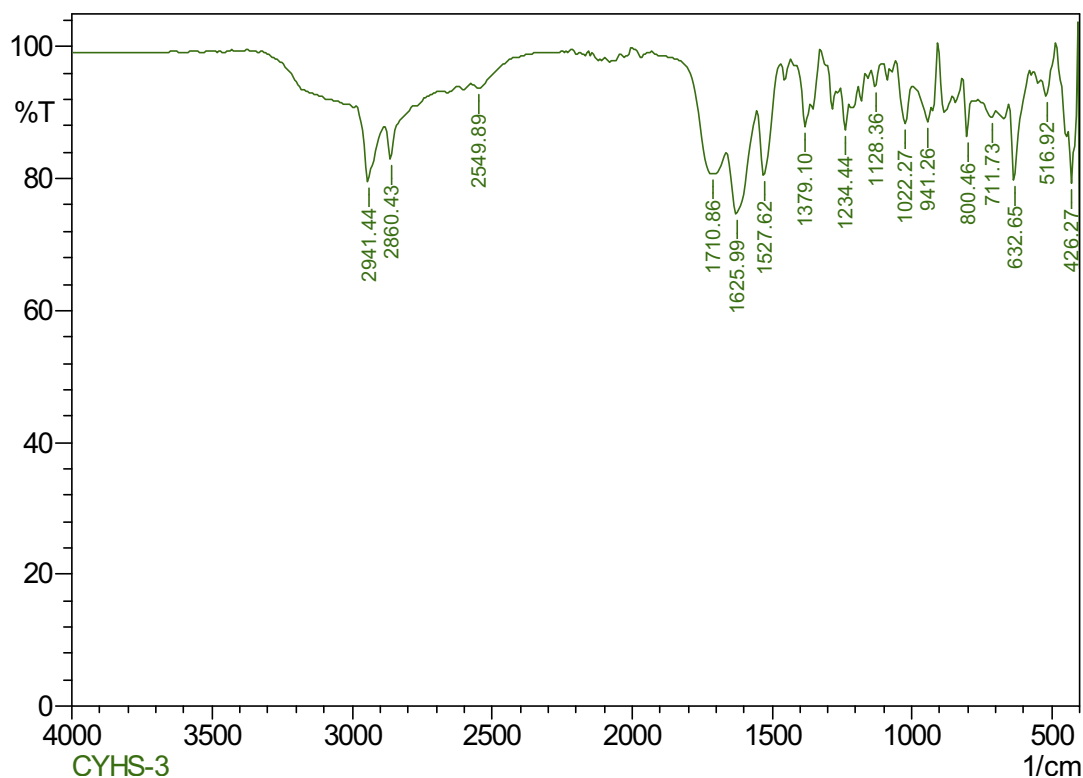


Fig. 2. FT-IR spectrum of BCSSA.

out as a function of frequency (200 Hz–5 MHz) in the temperature range of 40–80 °C. The suitable transparent crystal of thickness 0.89 mm and area of cross section 55 mm² was selected and its opposite faces were coated with silver paste, placed between two nickel electrode to ensure good electrical contact. The dielectric constant was calculated using the formula,

$$\epsilon_r = \frac{Cd}{\epsilon_0 A} \quad (10)$$

where, ϵ_r is the dielectric constant of the material, ϵ_0 is the permittivity of free space ($8.854 \times 10^{-12} \text{ F/M}$), A is the area of the crystal and t is the thickness of the sample.

The imaginary part of dielectric constant is calculated from the formula,

$$\epsilon'' = \epsilon' \tan \delta \quad (11)$$

here, ϵ' is real part of the dielectric constant and $\tan \delta$ is dielectric loss which was measured directly from the impedance analyzer. The dielectric constant and dielectric loss were plotted as a function of frequency. From Fig. 4 (a) and (b), it is clear that the dielectric constant (ϵ_r) and dielectric loss ($\tan \delta$) decrease with increase in frequency. At low frequency region the high value of dielectric constant and dielectric loss are due to the presence of all types of polarization namely space charge, ionic electronic and orientational polarizations. The decreasing nature is due to the loss of these polarizations significantly and almost constant at higher frequency region. The low value of loss suggest that the crystal potentially applicable for the fabrication of nonlinear device and electro-optic applications.

The AC conductivity was calculated using the formula [17],

$$\sigma_{ac} = 2\pi f \epsilon_0 \epsilon_r \tan \delta \quad (12)$$

where, f is the frequency of applied field. The plot of AC conductivity versus frequency and AC resistivity versus frequency at different temperature (40–80 °C) are shown in Fig. 5 (a) and (b). It is clear that the conductivity increases and resistivity decreases with increase in frequency. Due to thermal expansion the AC conductivity decreased with increase in the temperature [18].

According to the Arrhenius relation the variation of AC conductivity with temperature is given by $\sigma_{ac} = \sigma_0 \exp\left(\frac{-E_a}{RT}\right)$, where K is the Boltzmann constant, E_a is the activation energy and T is absolute temperature. The activation energy was calculated by

plotting the graph between $\ln \sigma_{ac}$ and $1000/T$ is given in Fig. 5 (c). The slope of the graph is used to calculate the activation energy using the relation $E_a = -\text{slope} \times 1000 \times K$. The activation energy at 10 KHz, 100 KHz and 1 MHz is 0.77 eV, 0.48 eV and 0.28 eV respectively.

3.5. Impedance analysis

Impedance spectroscopy is a powerful tool to analyze the electrical property and relaxation mechanism in the material. Real and imaginary parts of complex impedance were calculated using the relation, $Z' = Z \cos \theta$ and $Z'' = Z \sin \theta$ [19]. Fig. 6 (a) and (b) represents the variation of real and imaginary part of impedance with frequency. It shows that the Z' value decreases with increase in frequency represents the increasing conductivity with frequency. Initially the value of Z'' increases with frequency and at particular frequency known as relaxation frequency it reaches maximum value. Further decreasing value of Z'' implies the presence of relaxation occurs due to the immobile charges present in the material [20].

The dc electrical conductivity of BCSSA was evaluated using the formula,

$$\sigma_{dc} = \frac{d}{AR_{dc}} \quad (13)$$

where, d is the thickness of the crystal, A is area of the crystal and R_{dc} is total electrical resistance of the sample which was evaluated from Cole-Cole plots plotted between Z' and Z'' . The Cole-Cole plot at different temperature (40–80 °C) of BCSSA is shown in Fig. 6 (c) and the obtained value of resistance, capacitance and relaxation time are tabulated in Table 3.

3.6. Third order nonlinear optical studies

Z-scan technique is a versatile tool to measure the magnitude and sign of nonlinear refractive index and nonlinear absorption coefficient of the materials [21]. Z scan technique was carried out using CW Nd:YAG Laser at 532 nm with 3.5 cm focal length of lens. The beam waist (ω_0) was calculated at the focus and it is 15.84 μm . The CYHC crystal of 1 mm thickness was translated through the axial direction that is the direction of laser beam propagation. The variation of transmittance intensity was calibrated with respect to the Z which is useful to draw open and closed aperture curve. Fig. 7 (a), (b) and (c) show the open, closed and ratio of closed to open aperture Z scan curves. The irradiance of Gaussian beam increases

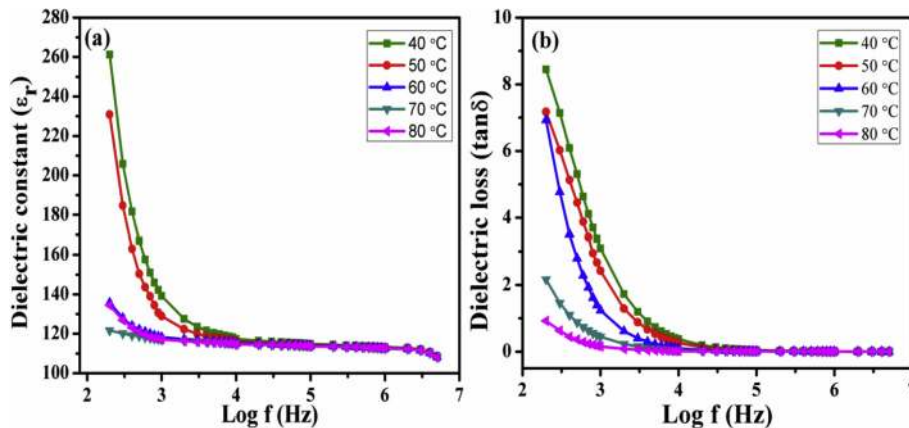


Fig. 4. (a) Dielectric constant and (b) dielectric loss of BCSSA crystal.

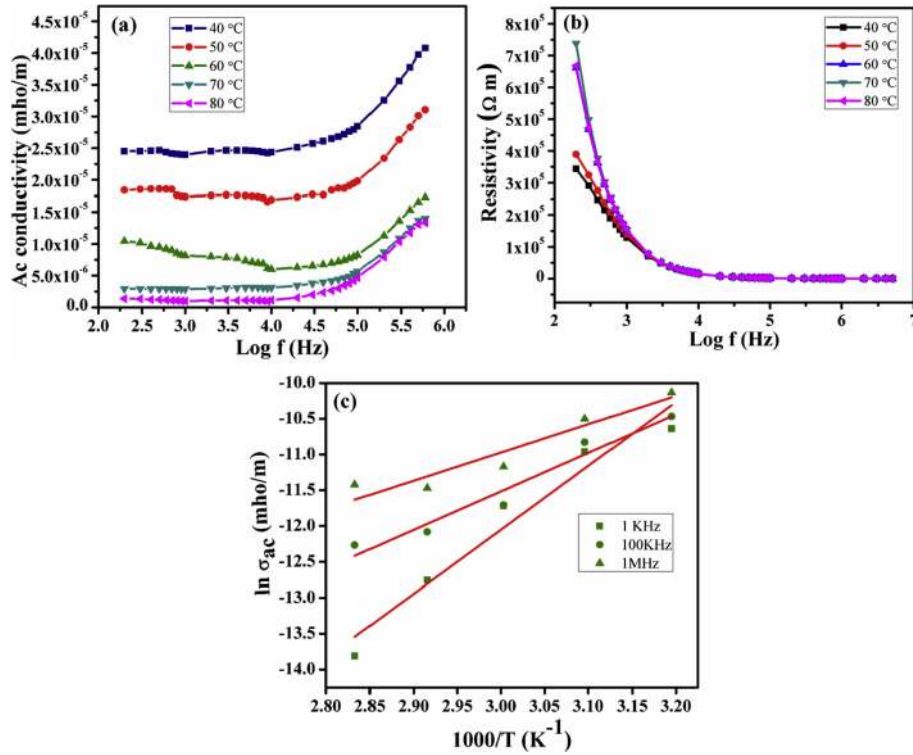


Fig. 5. (a) AC conductivity. (b) resistivity of BCSSA crystal and (c) $1000/T$ vs $\ln \sigma_{ac}$ spectrum.

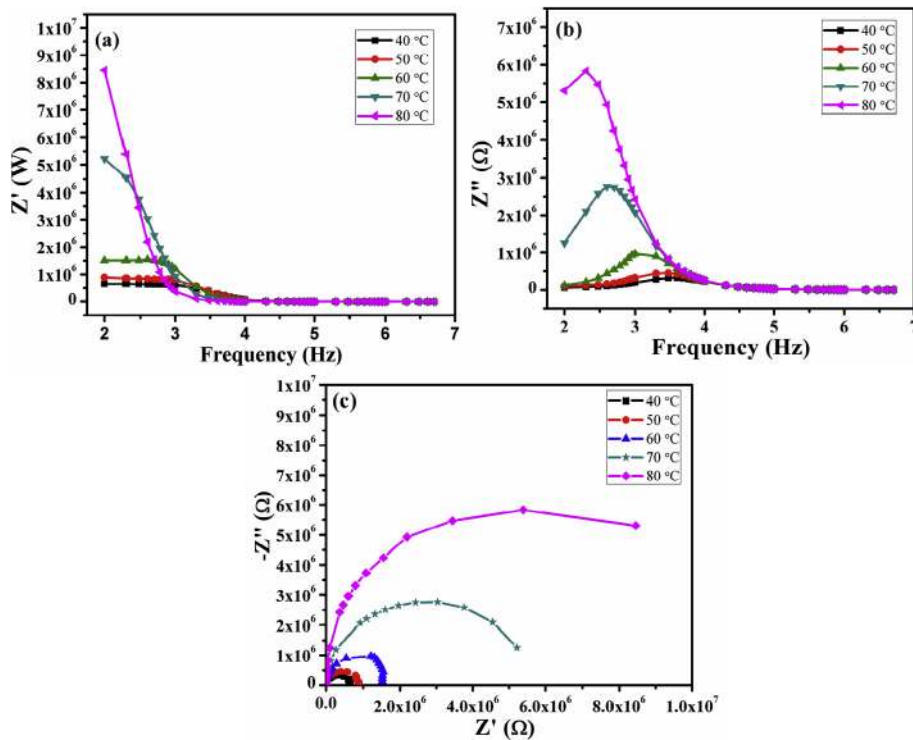


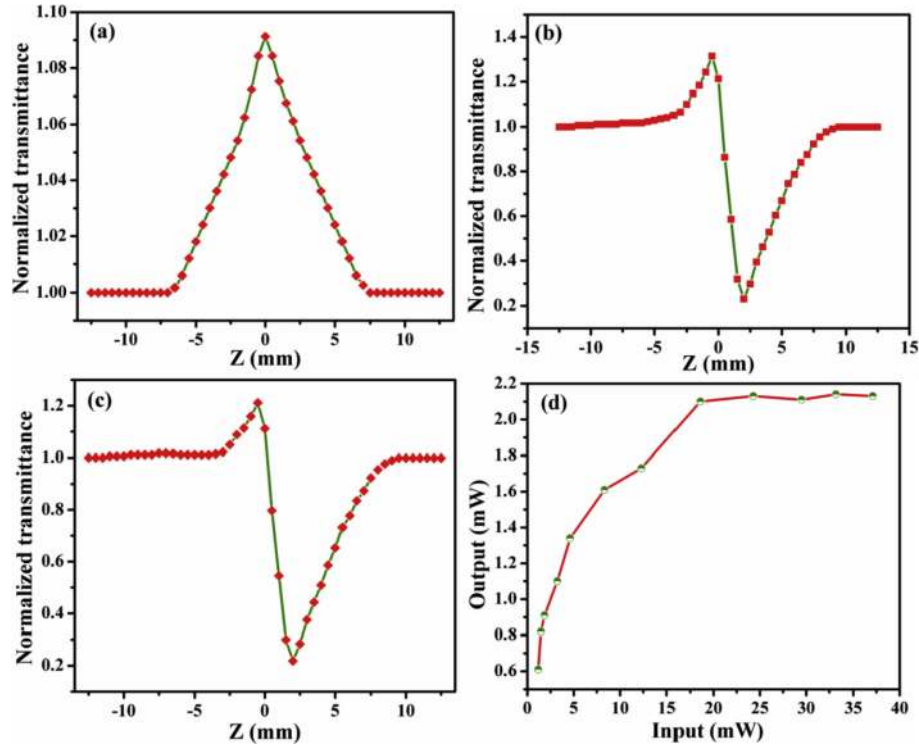
Fig. 6. Variation of (a) real and (b) imaginary part of impedance with frequency and (c) Cole-Cole plot for BCSSA crystal.

or decreases depends on the absorption and refractive index of the material which is act as a thin lens of variable focal length. From Fig. 7 (a), the transmittance increases at the focus ($Z = 0$) indicates the saturation absorption (SA) in the BCSSA crystal. From Fig. 7 (b),

the pre focal transmittance maximum (peak) followed by the post focal transmittance minimum (valley) configuration clearly suggest the sign of nonlinear refractive index is negative which is attributed to self-defocusing effect. This may be caused by the local variation

Table 3
Conductance parameters.

Temperature (° C)	$R_g \times 10^5 (\Omega)$	F_g (Hz)	C_g (F)	τ (s)	$\sigma_{dc} \times 10^{-5}$ (S cm ⁻¹)
40	6.5	4000	6.12×10^{11}	3.98×10^{-5}	2.4
50	8.6	3000	6.17×10^{11}	5.37×10^{-5}	1.8
60	15.01	1000	1.06×10^{11}	1.59×10^{-4}	1.0
70	54.04	400	7.36×10^{11}	3.98×10^{-4}	0.29
80	103.59	200	1.47×10^{10}	7.96×10^{-4}	0.15

**Fig. 7.** (a) Open aperture curve. (b) closed aperture curve. (c) ratio of closed to open aperture curve and (d) optical limiting behavior of BCSSA.

of refractive index with temperature [22]. On-axis phase shift ($\Delta\Phi$) calculated as the function of peak and valley transmittance is given by

$$\Delta T_{p-v} = 0.406(1 - S)^{0.25} |\Delta\Phi| \quad (14)$$

here, S is aperture linear transmittance which is found from the relation $S = 1 - \exp(-2r_a^2/\omega_a^2)$, where r_a is the radius of the aperture and ω_a is beam radius at the aperture. Third order nonlinear refractive index was calculated using [23],

$$n_2 = \frac{\Delta\Phi}{KI \cdot L_{eff}} \quad (15)$$

where, L_{eff} is an effective thickness of the crystal and it was calculated using the following relation $L_{eff} = \frac{1 - \exp(-\alpha L)}{\alpha}$ and K is the wave number ($K = 2\pi/\lambda$). I_0 is the intensity of the laser beam, α and L is linear absorption and thickness of the sample respectively. The nonlinear absorption coefficient (β) was determined using the formula [24],

$$\beta = \frac{2\sqrt{2}\Delta T}{I_0 L_{eff}} \quad (16)$$

where, ΔT is the valley value at the open aperture curve. The third

order nonlinear optical susceptibility was calculated using the relation [25],

$$|\chi^{(3)}| = \left[\left(\text{Re}(\chi^{(3)}) \right)^2 + \left(\text{Im}(\chi^{(3)}) \right)^2 \right]^{1/2} \quad (17)$$

The real and imaginary part of third order susceptibility were obtained from the expressions [26],

$$\text{Re}(\chi^{(3)}) esu = \frac{10^{-4} \epsilon_0 C^2 n_0^2 n_2}{\pi} \text{cm}^2 \text{W}^{-1} \quad (18)$$

$$\text{Im}(\chi^{(3)}) esu = \frac{10^{-2} \epsilon_0 C^2 n_0^2 \lambda \beta}{4\pi^2} \text{cm}^2 \text{W}^{-1} \quad (19)$$

where, c is the velocity of light, n_0 is the linear refractive index and λ is the wavelength of the laser beam. The obtained value of nonlinear refractive index, nonlinear absorption coefficient and nonlinear optical susceptibility of BCSSA crystal are $-4.718 \times 10^{-8} \text{ cm}^2/\text{W}$, $0.061 \times 10^{-4} \text{ cm/W}$ and $2.274 \times 10^{-6} \text{ esu}$ respectively. Third order nonlinear susceptibility was compared with some organic crystals (Table 4). Optical limiting behavior of BCSSA crystal was tested using Nd:YAG Laser (1064 nm 50 mW) and is shown in Fig. 7 (d). The transmitted output intensity is varying linearly with low input intensity and at high incident intensities it

Table 4
Comparison of χ^3 with some organic crystals.

S. No	Crystal	Third order optical susceptibility χ^3 (esu)	Reference
1	PBS	8.1787×10^{-7}	[28]
2	NTF	-1.844×10^{-6}	[29]
3	CYHPH	3.641×10^{-8}	[30]
4	UPN	2.8337×10^{-12}	[31]
5	BCSSA	2.274×10^{-6}	Present work

starts to deviate nonlinearly, while increasing the intensity it reaches plateau and is saturated at a point which is called limiting amplitude. The limiting threshold for saturation and output clamping values are found to be 18.5 mW and 2.1 mW respectively. Hence this material is suitable for nonlinear optical applications such as the protection of human eyes and photo sensors [27].

3.7. Chemical etching studies

Nonlinear optical properties depend on the crystalline perfection. Chemical etching studies discuss the crystal defects and its growth mechanism (spiral, rectangular, hillocks and step pattern etc.) in detail [32]. BCSSA surface was polished and etched in methanol solution at room temperature with 30 s etching time. Then the surface etchant was dried gently and Fig. 8 shows before and after the etched pattern (30 s) of BCSSA crystal. It confirms the layer growth and two dimensional nucleation mechanisms and a rectangular pattern also was observed at 30 s. The location of growth center depends on supersaturation, temperature and crystal face etc. When the supersaturation of crystal growth surface at some points is higher than other parts, then they act as a centre of repeated two dimensional nucleation spread on the growing surface [33].

4. Conclusion

Third order organic nonlinear optical crystal of bis(cyclohexylammonium) succinate succinic acid was grown by slow evaporation technique and using slow cooling technique, the dimension of $26 \times 9 \times 3 \text{ mm}^3$ was harvested from the solution. The cell parameters of BCSSA are $a = 9.640$ (2) (Å), $b = 10.514$ (11) (Å), $c = 11.433$ (2) (Å), $\alpha = 96.76$ (4)°, $\beta = 93.38$ (2)°, $\gamma = 90.99$ (5)° and the volume (V) is 1147.6 (3) (Å³). The functional group present in the compound was confirmed using FT-IR analysis and optical band gap of BCSSA was found to be 4.9 eV. The low dielectric loss reveals less defect concentration with enhanced optical quality that

supports nonlinear optical application. The activation energy of BCSSA crystal was calculated at the frequency range of 10 KHz, 100 KHz and 1 MHz (0.77 eV, 0.48 eV and 0.28 eV respectively). Nonlinear refractive index ($-4.718 \times 10^{-8} \text{ cm}^2/\text{W}$) and nonlinear absorption coefficient ($0.061 \times 10^{-4} \text{ cm/W}$) were calculated from Z scan technique. Saturation absorption and self-defocusing effect was observed in BCSSA crystal. The optical limiting response was tested, limiting threshold value and clamping values are found to be 18.5 mW and 2.1 mW respectively and also chemical etching studies were carried out for this compound. It can hence be concluded that the BCSSA crystal is a potential material for nonlinear optical applications.

Acknowledgements

The authors are thankful to the VIT University for providing excellent lab facility and one of the authors R.G thanks to VIT management for providing Research Associateship. We thank Dr. G. Vinitha, VIT University, Chennai for Z-scan analysis.

References

- [1] L. Jiang, H. Dong, W. Hu, J. Mater. Chem. 20 (2010) 4994.
- [2] T. Kaino, J. Opt. A Pure Appl. Opt 2 (2000) R1.
- [3] M.R. Ramanan, R. Radhakrishnan, T. Dhanabal, M. Sivaraju, R. Ashokkumar, Optik 126 (2015) 5600.
- [4] B. Babu, J. Chandrasekaran, R. Thirumurugan, V. Jayaramkrishnan, K. Anitha, J. Mater. Sci. Mater. Electron. 28 (2017) 1124.
- [5] S. Basu, Ind. Eng. Chem. Prod. Res. Dev. 23 (1984) 183.
- [6] T. Jayanalina, G. Rajarajan, K. Boopathi, K. Sreevani, J. Cryst. Growth 426 (2015) 9.
- [7] S. Krishnan, C.J. Raj, S.J. Das, J. Cryst. Growth 310 (2008) 3313.
- [8] D. Kalaivani, D. Arthi, A. Mukunthan, D. Jayaraman, V. Joseph, J. Cryst. Growth 426 (2015) 135.
- [9] M. Sarr, A. Dlasse-Sarr, L. Diop, L. Plasseraud, H. Cattey, Acta Cryst. E71 (2015) 899.
- [10] F.A. Najjar, G.B. Vakili, F.A. Wani, F.A. Mir, K. Asokan, 26 (2015) 1455.
- [11] P. Karupppasamy, V. Sivasubramani, M.S. Pandian, P. Ramasamy, RSC Adv. 6 (2016), 109105.
- [12] N.S. Sowmya, S. Sampathkrishnan, S. Sudhahar, M.K. Kumar, R.M. Kumar, Optik 127 (2016) 3024.
- [13] R. Padmapathy, N. Karthikeyan, D. Sathya, R. Jagan, R.M. Kumar, K. Sivakumar, RSC Adv. 6 (2016) 68468.
- [14] G.A. Babu, P. Ramasamy, Mater. Chem. Phys. 119 (2010) 533.
- [15] P.K. Devi, K. Venkatachalam, Mater. Chem. Phys. 183 (2016) 210.
- [16] M. Shkir, I.S. Yahia, A.M.A. Al-Qahtani, Mater. Chem. Phys. 184 (2016) 12.
- [17] F. Helen, G. Kanchana, Mater. Chem. Phys. 151 (2015) 5.
- [18] M.P. Binitha, P.P. Pradyumnan, Indian J. Phys. 88 (2014) 497.
- [19] B. Uma, K.S. Murugesan, S. Krishnan, R. Jayavel, B.M. Boaz, Mater. Chem. Phys. 142 (2013) 659.
- [20] T. Badapanda, R.K. Harichandan, S.S. Nayak, A. Mishra, S. Anwar, P. Appl. Ceram. 8 (2014) 145.
- [21] A.N. Prabhu, V. Upadhyaya, A. Jayarama, K.S. Bhat, Mater. Chem. Phys. 138 (2013) 179.
- [22] T.C.S. Girisun, S. Dhanuskodi, D. Mangalaraj, J. Phillip, Curr. Appl. Phys. 11 (2011) 838.
- [23] M.D. Bharathi, G. Ahila, J. Mohana, G. Chakkaravarthi, G. Anbalagan, Mater. Chem. Phys. 192 (2017) 215.
- [24] M. Saravanan, Opt. Mater. 58 (2016) 327.
- [25] N. Sudharsana, B. Keerthana, R. Nagalakshmi, V. Krishnakumar, L.G. Prasad, Mater. Chem. Phys. 134 (2012) 736.
- [26] F.Z. Henari, W.J. Blau, L.R. Milgrom, G. Yahioğlu, D. Phillips, J.A. Lacey, Chem. Phys. Lett. 267 (1997) 229.
- [27] M. Saravanan, T.C.S. Girisun, Mater. Chem. Phys. 160 (2015) 413.
- [28] S. Kalaiyarasi, I. MD Zahid, S.R. Devi, R.M. Kumar, J. Cryst. Growth 460 (2017) 105.
- [29] P.V. Dhanaraj, N.P. Rajesh, J.K. Sundar, S. Natarajan, G. Vinitha, Mater. Chem. Phys. 129 (2011) 457.
- [30] R. Gomathi, S. Madeswaran, D.R. Babu, J. Mater. Sci. Mater. Electron. 28 (2017) 11374.
- [31] S. Selvakumar, A.L. Rajesh, J. Mater. Sci. Mater. Electron. 27 (2016) 7509.
- [32] G.H. Sun, G.H. Zhang, X.Q. Wang, Z.H. Sun, D. Xu, Mater. Chem. Phys. 122 (2010) 524.
- [33] K. Sangwal, Etching of Crystals, North-Holland Physics Publishing, Amsterdam, The Netherlands, 1987.

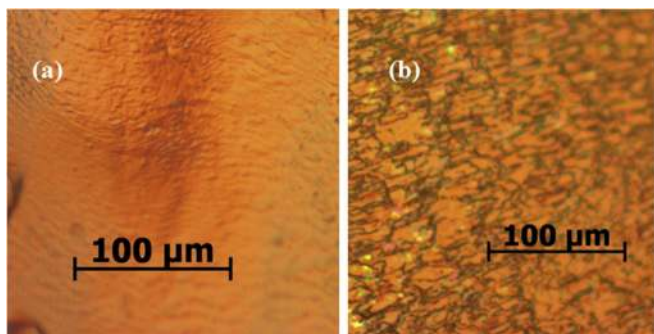


Fig. 8. Etch pattern (a) before and (b) after etching (30 s).